Particle Motion in Packed/Ebullated Beds by CT and CARPT

Jinwen Chen, Novica Rados, Muthanna H. Al-Dahhan, and Milorad P. Duduković
Dept. of Chemical Engineering, Washington University in St. Louis, St. Louis, MO 63130

Duyen Nguyen and Krishniah Parimi
Chevron Research and Technology Co., Richmond, CA 94802

Computed tomography (CT) and computer-automated radioactive particle tracking (CARPT) were used to study the gas distribution and incipient particle motion in a packed/ebullated bed in which gas and liquid are in cocurrent upflow. CT scans were performed to evaluate the gas–liquid distributor and gas sparger for the experiments. Using a perforated plate gas–liquid distributor (with 96 1-mm holes, open area of 0.1%) and a gas sparger (cross-shaped, with 16 3-mm holes), the cross-sectional gas holdup distribution in the packed/ebullated bed was relatively uniform, with gas holdup of about 0.11 in the center and 0.09 near the wall of the bed at superficial gas and liquid velocities of 2 and 0.3 cm/s, respectively. The cross-sectional averaged gas holdup was 0.095. CARPT experiments were utilized in an air–water–ethanol– (10 wt. %) solids system to identify the operating conditions at which solid particles first start to move in the bed. At a superficial gas velocity of 1.7 cm/s and superficial liquid velocity of 0.3 cm/s, solids particles in the bed started to move and travel long distances in the axial direction. CARPT experiments in the same system at superficial gas velocity of 2.0 cm/s and superficial liquid velocity of 0.3 cm/s showed that the solid particles in the bed were moving significantly throughout the column, generating a recirculation pattern with upflow in the center and downflow near the wall of the column. The time-averaged maximum upward and downward velocity of the tracer particle was about 0.47 and 0.57 mm/s, respectively.

Introduction

Gas–liquid–solid packed/ebullated beds are widely used in petroleum, chemical, food, and environmental processes. One of the operation modes in these processes is that gas and liquid flow upward through a packed-bed of solids particles that are essentially stationary. Generally, the gas and liquid phases are introduced through a distributor/sparger either together or separately. The design of the distributor/sparger is critical for the distribution and flow pattern of the gas and liquid phases in the bed. A perforated plate distributor is a metal plate, while a sparger can be made in different shapes (such as ring, cross). Both the distributor and sparger have small holes for distribution of only the gas or both the gas and liquid phases. In some operations, the bed is subject to periodic withdrawals of a small batch of particles and replenishment with fresh ones. Stationary particles (during normal operation of the bed) and plug flow of solids (during withdrawal and replenishment) are most desirable from the operational point of view. It is thus necessary to determine whether any backmixing of solids occurs in the bed during normal operation. It is important to identify the operating conditions at which incipient particle motion occurs and when the catalyst particles start to migrate throughout the bed. It is also of interest and importance to determine the magnitudes of the traveling velocity of solid particles when migration occurs. This type of study has not been accomplished before due to the lack of reliable experimental techniques.

Correspondence concerning this article should be addressed to M. H. Al-Dahhan.
Current address of J. Chen: National Center for Upgrading Technology, 1 Oil Patch Drive, Devon, AB T9G 1A8 Canada.

In the past decade, a number of advanced techniques for noninvasive monitoring of multiphase flows have been developed. For velocity measurements, the techniques include particle image velocimetry (PIV) (Chen and Fan, 1992), laser Doppler anemometry (LDA) (Gross and Quhlman, 1992; Mudde et al., 1997), radioactive particle tracking (RPT) (Bascoul et al., 1993; Larachi et al., 1995), or computer automated radioactive particle tracking (CARPT) (Devanathan et al., 1990; Moslemian et al., 1992; Yang et al., 1993; Limtrakul, 1996; Roy et al., 1997; Degaleesan, 1997; Chen et al., 1998, 1999). Various kinds of densitometry and tomography/radiography have been applied to phase-density measurements, such as X-ray computed tomography (X-ray CT) (Kantzas, 1994), X-ray radiography (Yates et al., 1994; Yates, 1997), gamma-ray densitometry (Shollenberger et al., 1997, Mudde et al., 1999), gamma-ray-computed tomography (gamma-ray CT) (Kumar et al., 1995, 1997), and electronic impedance tomography (Halow, 1997). A detailed review on the applications of noninvasive techniques in monitoring of multiphase flow can be found in Chaouki et al. (1997).

The Chemical Reaction Engineering Laboratory (CREL) at Washington University in St. Louis has developed unique experimental facilities for quantification of phase density and velocity fields in multiphase flow systems. These include computer-automated radioactive particle tracking (CARPT) and computed tomography (CT). CARPT provides experimental data on instantaneous positions, time-averaged velocity profiles, and turbulent parameters in the entire flow fields (Devanathan et al., 1990; Moslemian et al., 1992; Yang et al., 1993), while CT yields the time-averaged density profiles at discrete cross-sectional planes of the reactor (Kumar, 1994; Kumar et al., 1995, 1997). The combination of CARPT with CT has been used to produce unique data in multiphase systems such as bubble columns (Degaleesan, 1997; Degaleesan et al., 1997; Chen et al., 1998, 1999), liquid–solid and gas–liquid–solid fluidized beds (Limtrakul, 1996), and liquid–solid risers (Roy et al., 1997). CARPT and CT are especially useful in providing information on opaque flow systems such as the ebullated bed.

The objective of this work was to determine if the incipient particle migration could be identified using CARPT. Specifically, it was desired to (1) evaluate by CT scans if the gas–liquid distributor and gas sparger used could achieve relatively uniform gas holdup distribution in the packed bed, (2) use the evaluated distributor and sparger to determine by CARPT the conditions at which solid particles first start to migrate through the bed, that is, identify the conditions for incipient particle motion, and (3) determine particle trajectories, mean velocities, and motion patterns when significant particle motion occurs.

Experimental Setup and Operating Conditions

Experimental setup

The packed-bed reactor used in this study is made of a Plexiglas pipe with an inner diameter of 30.5 cm. The solids phase consists of 3.2-mm alumina particles (Activated Alumina, ALCOA Industrial Chemicals). During the experiments, the packed height of the bed was kept at about 90 to 100 cm above the distributor ($L/D = 3 \sim 3.3$). The experimental setup is shown in Figure 1. The flow rates of both the gas phase (compressed air) and liquid phase (tap water or solution of 10 wt. % ethanol in tap water) are measured by rotameters. The gas and liquid phases, which are in cocurrent upflow in the bed, are introduced to a plenum that is located below the distributor. The gas is introduced via a cross-shaped sparger with 16 holes 3 mm in diameter, while the liquid phase is introduced via the inlet pipe connected to the plenum base. Both air and water flow upward through the holes in the distributor. The distributors investigated are perforated plates. Distributor I has 204 holes of 0.77 mm, of which 180 are distributed in 9 rings of 1.5 cm apart with 20 holes in each ring. The other 24 holes are equally distributed in the outer ring, which is also 1.5 cm apart from the adjacent ring. This yields a total open area of 0.13%. Distributor II has 96 holes 1 mm in diameter, yielding an open area of 0.1%. The holes are distributed in a triangular pattern. In addition, a gas sparger is used in the plenum with distributor II to improve the gas distribution before the gas flows up with the liquid to the bed through the distributor. The gas sparger consists of four stainless-steel tubes arranged as a cross. In each tube, there are two pairs of 3-mm holes that are located at 53 mm and 118 mm from the center of the cross. The two holes for each pair are positioned at 180 deg. During the experiments, all the holes in the gas sparger were pointing in the horizontal direction to get a more uniform gas distribution. An expanded section of the column (45.7 cm in diameter and 45.7 cm in height) was used on the top to separate the gas from the liquid. The gas is vented while the liquid flows to a tank for recycle.

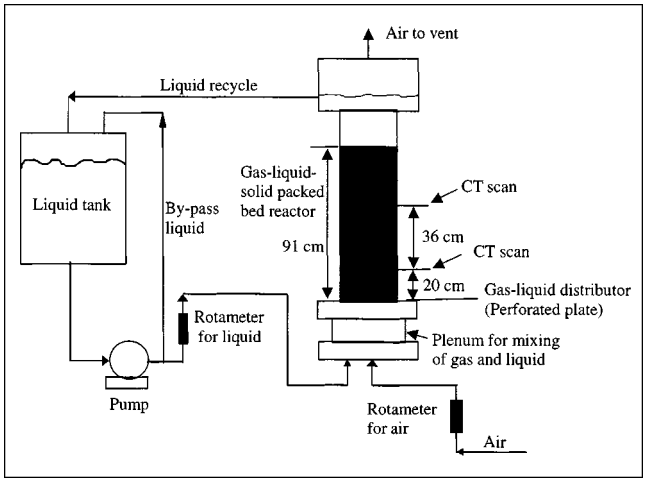

Figure 1. Experimental setup.

CT facility

The CT scanner in CREL is a third-generation fan-beam in-house gamma-ray scanner. The details of the hardware and software have been described elsewhere (Kumar, 1994; Kumar et al., 1995, 1997) and will be summarized here. The scanner consists of an array of collimated (opening size 5×10 mm) NaI (Tl) detectors of 5 cm in diameter (9 detectors were used for the present study to cover the whole cross section of the column) and a gamma-ray source (an encapsulated Cesium-137 with activity of about 92 mCi). The detectors and

the source are mounted on a plate that can be rotated, which makes it possible to get a 360° scan around the column. The whole assembly can be moved up and down to scan different axial levels of the column. This design of the CT scanner yields a spatial resolution of 3.5 mm in the horizontal direction and 10 mm in the vertical direction. In order to get statistically significant results and in order to reduce the position effect on the scans, CT scans were conducted around the whole cross section (360°) with a total scanning time of about 2 h.

The intensity of a beam of monoenergetic radiation that is transmitted through a homogeneous material can be expressed by the Beer-Lambert's law:

$$T = \frac{I}{I_0} = e^{-\rho\mu l}, \tag{1}$$

where T is the transmission ratio, I_0 is the incident radiation, I is the detected radiation, μ is the mass attenuation coefficient, ρ is the medium density, and l is the path length through the medium. If the medium is made of two materials with mass attenuation coefficients μ_1 and μ_2, densities ρ_1 and ρ_2, and thickness l_1 and l_2, respectively, the total attenuation A is

$$A = \rho_1 \mu_1 l_1 + \rho_2 \mu_2 l_2. \tag{2}$$

Because $l_1 = \epsilon_1 L$ and $l_2 = \epsilon_2 L$, where $L = l_1 + l_2$, then

$$A = \left[\rho_1 \mu_1 \epsilon_1 + \rho_2 \mu_2 (1 - \epsilon_1) \right] L. \tag{3}$$

The measured quantity $\ln(I_0/I)$ is equal to the integral sum of the attenuation through the material along the beam path. For tomography, attenuations are measured along a number of such beam paths through the object from different directions around it. Given a set of attenuation measurements, the density distribution (image) can be reconstructed by using a suitable reconstruction algorithm. In this work, the estimation–maximization (E–M) algorithm is used for image reconstruction. The details of the algorithm are provided elsewhere (Kumar, 1994).

As discussed earlier, with a single-source CT scanner, one can quantify the individual phase holdup only for a two-phase flow system. A dual-source CT scanner or some other diagnostic is needed to quantify the individual phase holdups for a three-phase flow system. However, for a gas–liquid–solid three-phase flow system, if the gas and liquid superficial velocities are not so high that a fixed-bed state can be assumed in the column (except at the very top of the bed), one can still evaluate the individual phase holdups (volumetric fraction) for each of the three phases by using several scans as discussed below.

For a three-phase system, Eq. (2) can be written as

$$A_{g-l-s,ij} = \left[\rho_g \mu_g \epsilon_{g,ij} + \rho_l \mu_l (1 - \epsilon_{g,ij} - \epsilon_{s,ij}) + \rho_s \mu_s \epsilon_{s,ij} \right] L_{ij}, \tag{4}$$

where A_{ij} is the total attenuation in the pixel ij, ρ_g, ρ_l, ρ_s are the densities, μ_g, μ_l, μ_s are the mass attenuation coefficients, $\epsilon_{g,ij}$, $\epsilon_{l,ij}$, $\epsilon_{s,ij}$ are the holdups (volumetric fractions) for the gas, liquid, and solid phases, respectively, and L_{ij} is the length along which a particular gamma ray beam passes through this pixel.

Similarly, for the same column containing a pure liquid, the column containing gas and solids, and the column containing liquid and solids, the following relationships hold for the total attenuation for the same pixel beam:

$$A_{l,ij} = \rho_l \mu_l L_{ij} \tag{5}$$

$$A_{g-s,ij} = \left[\rho_g \mu_g (1 - \epsilon_{s,ij}) + \rho_s \mu_s \epsilon_{s,ij} \right] L_{ij} \tag{6}$$

$$A_{l-s,ij} = \left[\rho_l \mu_l (1 - \epsilon_{s,ij}) + \rho_s \mu_s \epsilon_{s,ij} \right] L_{ij}. \tag{7}$$

Since $\rho_g \ll \rho_l$ or ρ_s, and μ_g, μ_l, μ_s are of the same order of magnitude, the attenuation caused by the gas phase is negligible. Thus, combining Eqs. 5, 6, and 7, one can get an estimate of solids holdup in the pixel ij:

$$\epsilon_{s,ij} = 1 - (A_{l-s,ij} - A_{g-s,ij})/A_{l,ij}. \tag{8}$$

Combining Eqs. 4, 5, 6, and 7 yields an estimate of local gas holdup:

$$\epsilon_{g,ij} = (A_{l-s,ij} - A_{g-l-s,ij})/A_{l,ij} \tag{9}$$

Liquid holdup is obtained from

$$\epsilon_{l,ij} = 1 - \epsilon_{g,ij} - \epsilon_{s,ij}. \tag{10}$$

Therefore, by scanning the same column filled only with the liquid phase, with the packed bed consisting of gas and solid phases, with the packed bed consisting of liquid and solid phases, and finally scanning the gas–liquid–solid system at the same position, the holdups for all the three phases can be obtained. This procedure can be used only if the same packed bed configuration is preserved in each of the runs. This is the case for the range of the operating conditions used in this study, since the expanded bed height remains unchanged (within 1 to 2% of the original bed height) in all experiments. In addition, to maintain the same quality of the solid phase in all experiments, the bed was first soaked in the liquid phase to fill the pores of the particles with the liquid phase and then the liquid from the bed voidage was drained prior to scanning the bed for the cases listed earlier.

CARPT facility

Details about the hardware and software for the CARPT facility can be found elsewhere (Devanathan, 1991; Degaleesan, 1997). For the present study, a radioactive scandium Sc46 particle (about 0.5 mm in diameter and 2.99 g/cm^3 in density with the activity of about 250 μCi) was embedded into an aluminum particle with a diameter of 3.2 mm. In order to match the density of the solid phase (alumina) that is to be monitored, an air void is created inside the aluminum particle so that the composite density (scandium–aluminum–air) is equal to the density of the solid particles (alumina) of 1.6 g/cm^3 when saturated with water. With the

same particle size and density as that of the solid phase, the radioactive tracer particle is able to successfully mimic the dynamic behavior of the particles. The intensity of the gamma rays emitted by the tracer particle is continuously monitored at a frequency of 50 Hz by an array of 16 NaI (Tl) scintillation detectors of 5 cm in diameter. The detectors are strategically located around the test section so that wherever the radioactive particle is, there are at least 3–4 detectors in different directions close to the particle. Except near the bottom of the column, where no detectors were mounted. In order to determine the exact position of the tracer particle at each instant, calibration is performed for all detectors, providing a relationship between the distance from the detector to the particle and the intensity count received by the detector. Using this calibration information and the intensities of radiation received by detectors during each sampling period, the instantaneous position of the particle is calculated by an inverse-mapping algorithm. The moving velocities of the particle are then obtained by time differentiation (Devanathan, 1991; Degaleesan, 1997).

As mentioned earlier, calibration for all the detectors is needed prior to the experiments to get the relationship between the intensity count received by a detector and a distance between the detector and the tracer particle. For a given source strength, the intensity of radiation (counts/s) received by a detector from the radioactive source decays exponentially with the distance between the detector and the source due to attenuation. For these experiments, the attenuation is also a complex function of the column geometry and the medium being traveled or the holdups of the three individual phases. Therefore calibration must be conducted for each operating condition (*in situ* calibration). Figures 2a and 2b illustrate the arrangement and axial position of the detectors. Calibration experiments for CARPT involve positioning the radioactive tracer particle at several hundred known locations throughout the column and measuring the intensity counts received by the detectors. A specially designed device is used for calibration in this study, whose details are described elsewhere (Degaleesan, 1997) and briefly outlined here. The device essentially consists of a frame that is fixed on the top flange of the expansion part of the column. A circular plate with a radial slot that passes through the center is placed between four guiding wheels that allow rotation of the plate around the axis of the column. Fixed on the plate and aligned over the radial slot is UniSlide control with a clamping device to hold a stainless-steel rod of 12 mm in diameter. The entire rod consists of two sections that can be screwed together with perfect alignment. At the end of these two sections another smaller aluminum rod, 15 cm long and 6 mm in diameter, is mounted to hold the radioactive particle on its tip. The calibration is conducted so that by using the UniSlide control knob to fix the radial position and the rotation of the plate to fix the azimuthal position, the rod is inserted inside the bed at one location to the lowest calibration level. Vertical, upward movement of the rod allows the axial positioning of the radioactive particle and calibration on the higher calibration levels. Once the calibration at the highest calibration point along that vertical line is completed the rod is taken out of the bed, repositioned radially and azimuthally and inserted at the next location to the lowest calibration level in the bed. The calibration device and procedure allow

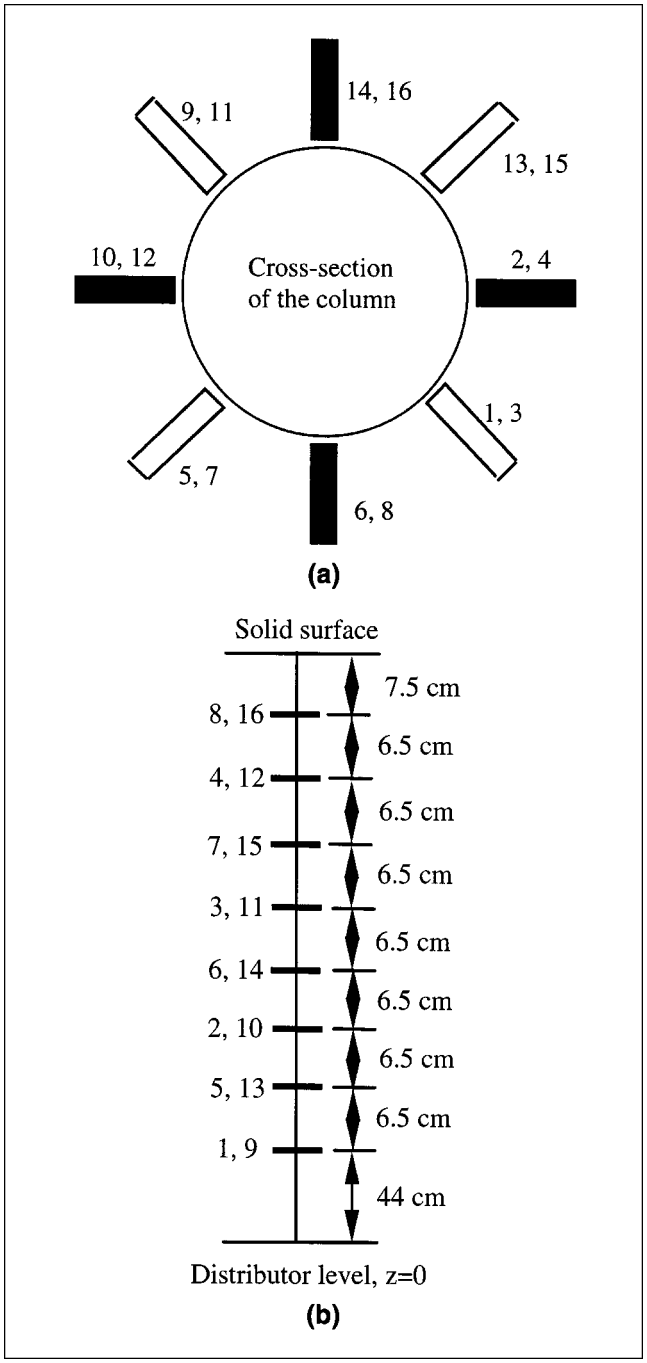

Figure 2. Detectors: (a) configuration; (b) axial levels.

for the precise placement of the radioactive particle to known locations in the column. The small thickness of the smaller rod of less than two particle diameters (6 mm vs. 3.2 mm) enables the axial rod movement with negligible altering of the bed packing.

In this study, a total of 901 calibration positions were employed to generate a fine three-dimensional mesh in the column. These 901 positions were equally distributed at 17 axial levels with 53 points at each level. For each of the detectors, the radiation counts (counts/s) and the distance between the

radioactive particle and the detector were acquired for all the calibration points. A cubic spline fitting method was used to obtain the calibration curves that are used to reconstruct the instantaneous positions of the tracer particle.

Evaluation of the Distributors/Sparger

Since the gas holdup distribution in the column is believed to drive the solids motion, it was necessary to check whether the gas holdup distribution in the bed is uniform. CT scans were conducted at the following conditions to evaluate the cross-sectional gas holdup distribution obtained with gas–liquid distributors I and II. For simplicity and the convenience of the experimental operation (no recycle is needed), filtered tap water instead of the ethanol–water solution has been used in the evaluation of the distributors. This simplification is safe since more uniform gas distribution is expected with the ethanol–water system because of smaller bubble sizes compared to the pure-water system.

Liquid: Filtered tap water
Gas: Compressed air
Total height of packed-bed: 91 cm from the distributor
Superficial gas velocity: 2 cm/s
Superficial liquid velocity: 0.3 cm/s
Axial levels for scanning: (1) 56 cm or $L/D = 1.84$ above the distributor; (2) 20 cm or $L/D = 0.66$ above the distributor.

Distributor I was investigated first. CT scanning results show that the cross-sectional gas holdup distribution obtained with this distributor is not quite uniform, with gas holdup of 0.13 in the center and 0.08 near the wall of the bed. This nonuniform distribution of gas holdup was not desired in the particle-tracking study. Therefore, distributor II together with the cross-shaped gas sparger was further evaluated using the CT scanning technique.

Figures 3a and 3b represent the cross-sectional gas- and solids-holdup distributions obtained with distributor II at an axial level of 56 cm ($L/D = 1.84$) from the distributor, respectively. Figure 4a shows the azimuthally averaged radial gas-holdup profiles at the two axial positions 56 and 20 cm from the distributor, while Figure 4b shows the azimuthally averaged radial solids-holdup profiles at the same axial positions. The gas and solid holdups are quite uniformly distributed in the cross section of the bed as seen from Figures 3a and 3b. The gas-holdup profiles are relatively flat at about 0.11 in the center and 0.09 at the wall of the column (see Figure 4a), giving a cross-sectional averaged gas holdup of about 0.095. The solid-holdup (volumetric fraction) profiles are also relatively flat except near the wall, where some artifact may exist due to the nonuniformity of the wall thickness and roundness and because of the spatial resolution (~ 3.5 mm) that is insufficient to fully capture the transition between the column interior and wall. The cross-sectional averaged solid holdup is about 0.66, which is within the range of 0.58 and 0.69 commonly reported in the open literature for lose and dense packed beds consisting of spherical particles.

Particle-Tracking Study Using CARPT

To identify the conditions (superficial gas and liquid velocities) at which the solid particles start to move in the packed bed with two-phase upflow, CARPT experiments were performed. The liquid phase used was ethanol (AAPER Alcohol and Chemical Co., 190 Proof – 95%)–water solution (10% of ethanol by weight) unless otherwise indicated. The concentration of ethanol in the solution was measured by an optical reflex meter (2WA-J, Shanghai, China) every 30 min and some ethanol was periodically added to the solution in order to keep the ethanol concentration constant during the experiments. Moreover, a fresh ethanol solution was always prepared and used after 24 h. The total height of the solids packed bed was kept at 97 cm from the distributor for all the CARPT experiments.

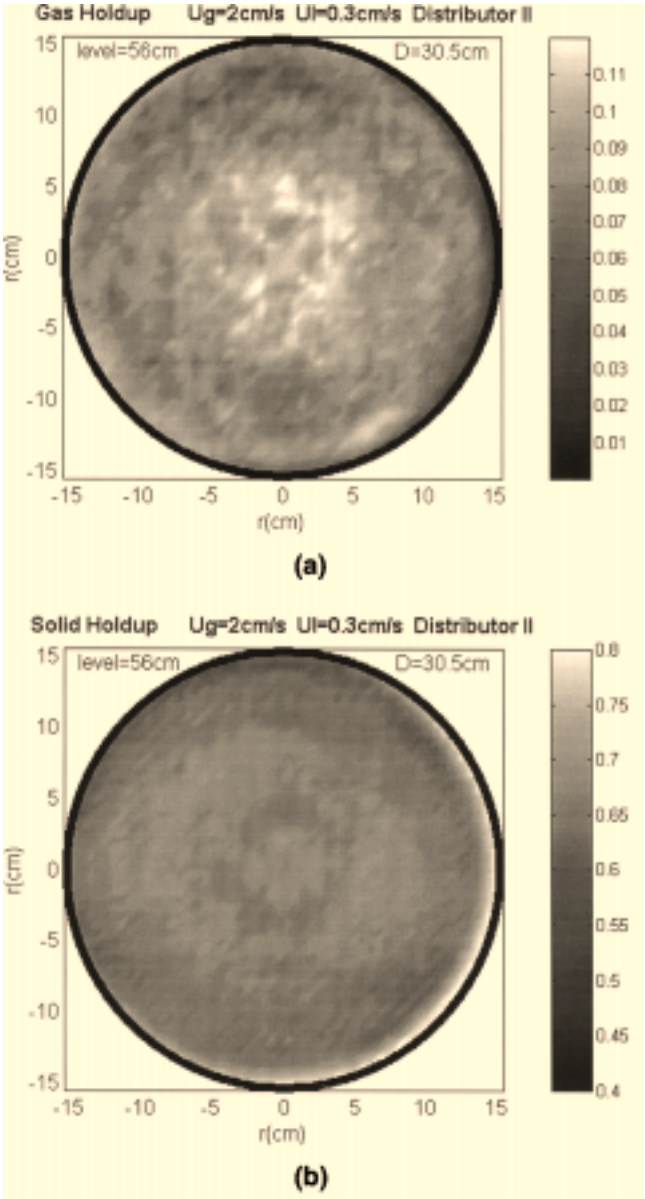

Figure 3. Time-averaged gas and solids cross-sectional distribution in the 30.5-cm-dia. packed-bed reactor.

Distributor II, $U_g = 2$ cm/s, $U_l = 0.3$ cm/s, air–water–alumina, two-phase upflow: (a) cross-sectional gas-holdup distribution; (b) cross-sectional solids-holdup distribution.

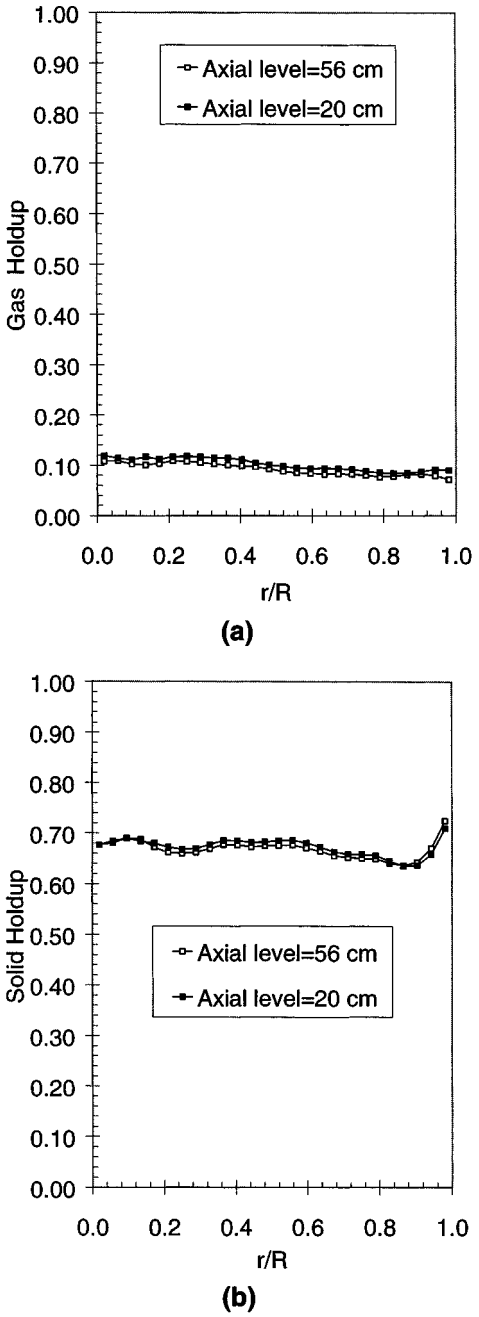

Figure 4. Radial gas- and solids-holdup (volumetric fraction) profiles in the 30.5-cm-dia. packed-bed reactor.

Distributor II, $U_g = 2$ cm/s, $U_l = 0.3$ cm/s, air–water–alumina, two-phase upflow: (a) radial gas holdup profiles; (b) radial solids-holdup profiles.

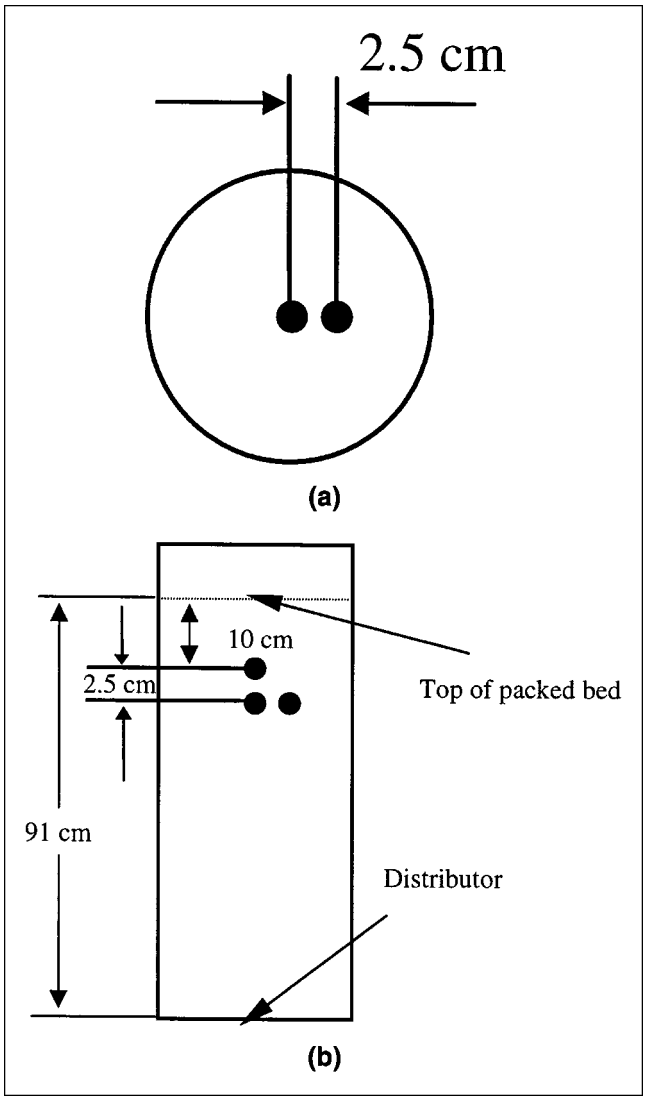

Figure 5. Three particle positions: (a) top view; (b) side view.

Preliminary CARPT experiments

There are 16 detectors mounted around the column (the lowest two detectors were 44 cm above the distributor). If the radioactive particle is not moving in the bed, the radiation counts detected by the detectors should be constant with time. In other words, if the radiation counts received by the detectors vary with time, the particle must be moving in the bed. This was verified by checking the radiation counts received by the detectors for a water-filled packed bed in which the radioactive particle, fixed at the tip of a 12.7-mm stainless-steel rod, was placed at three different positions. The three positions used were as follows (see Figures 5a and 5b):

Position 1: center of the column, 10 cm below the solids free surface

Position 2: center of the column, 12.5 cm below the solids free surface

Position 3: 2.5 cm from the center of the column, 12.5 cm below the solids free surface.

Figures 6a and 6b illustrate the radiation counts received over 30 min for the three radioactive-particle positions for detector 3 and detector 8, respectively. Detector 3 was placed at an axial position of 27 cm below the solids free surface, while detector 8 was placed at an axial position of 7.5 cm below the solids free surface and 45° away azimuthally from detector 3 (see Figure 2). It is obvious that (1) the intensity counts are constant with time, and (2) both of the two detectors can easily distinguish different positions of the particle.

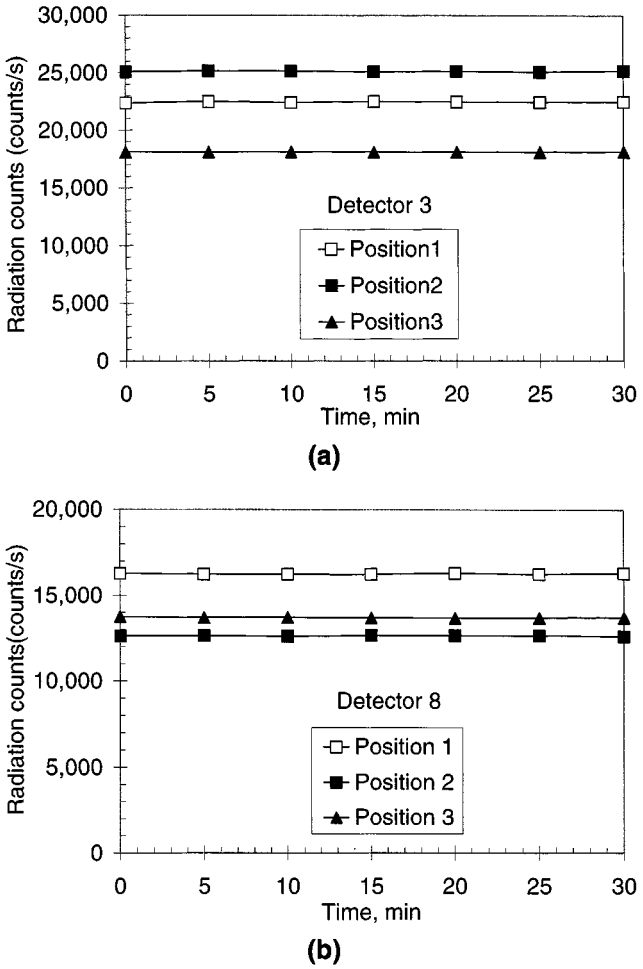

Figure 6. Radiation counts with time for different particle positions obtained with air–water–alumina system: (a) detector 3; (b) detector 8.

In other words, if the tracer particle moves by 2.5 cm from its original position, there will be a significant change in intensity counts for each detector.

In order to identify the conditions at which the solid particles start to move in the bed, experiments were conducted by releasing the particle into the bed and collecting the radioactive emissions at all the detectors. Different runs were performed by increasing the superficial gas velocity while keeping the superficial liquid velocity the same (0.3 cm/s). The radioactive particle was originally placed at a position which is 47 cm above the distributor and 8 cm from the center of the column. Figures 7a and 7b display the intensity counts received by four of the detectors over 1 h at superficial gas velocities of 1.5 cm/s and 1.7 cm/s, respectively. At 1.5 cm/s superficial gas velocity (Figure 7a), the intensity counts received by the four detectors are essentially constant. Only slight oscillations are observed at closer scrutiny (by expanding the time scale), but there is no long time drift in intensities. This implies that while the particle may be periodically moving, its movement is oscillatory in character and confined to at most one or two particle positions around its center. However, long-term changes in intensity counts with time can be observed at a superficial gas velocity of 1.7 cm/s for the

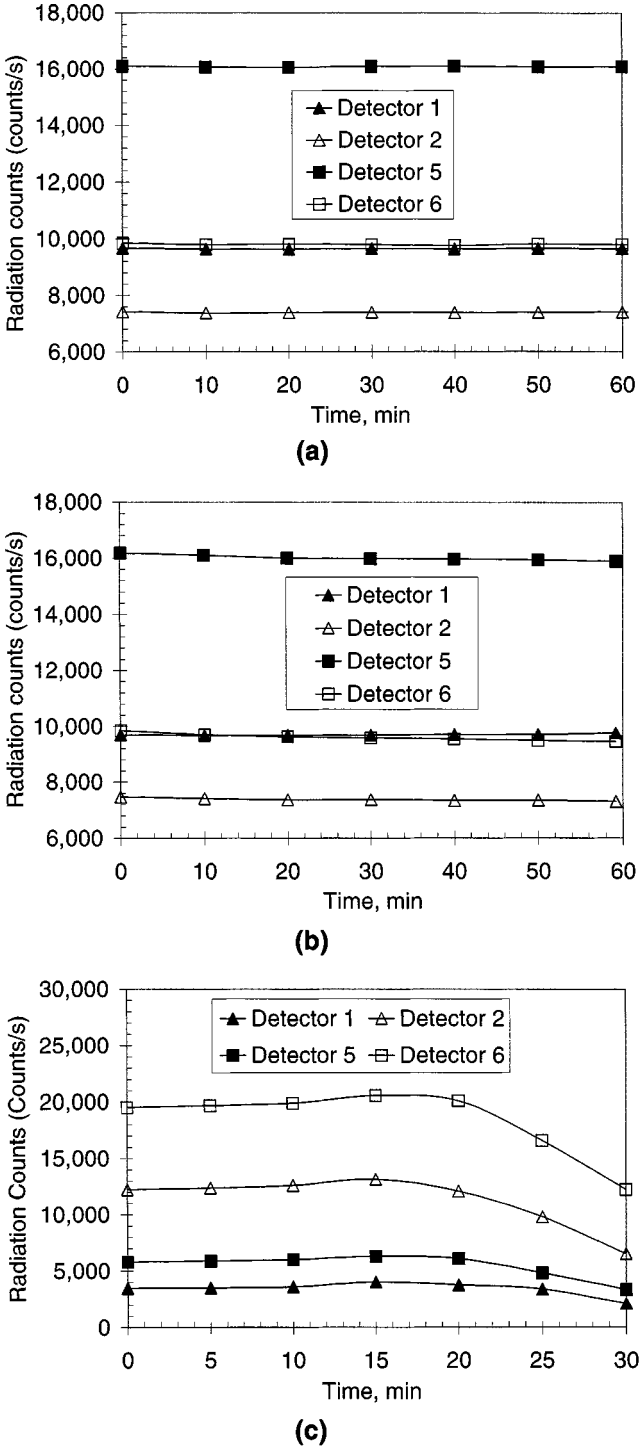

Figure 7. Intensity counts with time.

Distributor II, $U_l = 0.3$ cm/s, air–water + ethanol, two-phase upflow. Superficial gas velocity: (a) 1.5 cm/s; (b) 1.7 cm/s; (c) 2.0 cm/s.

same detectors as shown in Figure 7b, indicating that the particle is now definitely starting to slowly migrate through the bed. Thus, this operating condition can be considered as the one at which incipient long-distance particle movement occurs. As expected, at a superficial liquid velocity of 0.3 cm/s and superficial gas velocity of 2.0 cm/s, the particles now

move significantly inside the bed, as seen in Figure 7c, where the particle is moving, noticeably covering a long distance after 15 min of the experiment.

Results and discussion of CARPT experiments

After calibration, CARPT experiments can be run to measure particle motion. This was done by placing the radioactive particle in some position in the bed and running the experiment for over 20 h to collect sufficient data. However, since the particle moves very slowly in the bed, the particle cannot visit most parts of the column, even in 20 h. Two different initial particle positions were used: one was in the center of the column and 20 cm below the solid free surface, and the other one was 4 cm from the column wall and 20 cm below the solid surface. It should be noted that the original position of the particle is not important, since the particle can move anywhere in the column during the experiments.

Figures 8a and 8b show typical trajectories of the particle over 1 h. The particle's original position was in the center of the column and 20 cm below the free solid surface. Figure 8a represents the *z*-trajectory (axial position) of the particle, while Figure 8b presents the *x* and *y* trajectories (cross-sectional position) of the particle. The origin of the coordinates is the center of the distributor. It is obvious that the particle is moving throughout the column. It takes about 30 min for the particle to move from the top to the bottom (20 cm above the distributor) of the bed, indicating an axial migrating velocity of about 0.43 mm/s during this particular time period. Compared with axial movement, the radial movement of the particle is much less pronounced, as evident from Figure 8b.

In order to get the particle velocity, the whole bed was divided into fictitious cells, and particle position at each sample time was identified and assigned to a cell using the CARPT calibration curves. There were 50 divisions in the axial direction of the bed with 96 cells at each division, yielding 4,800 cells for the whole bed. An instantaneous velocity was assigned to a cell that contains the mean particle position between two successive locations. The instantaneous velocities were then averaged in each cell over the whole time span of the CARPT experiments to get the time-averaged particle velocities (the number of particle occurrences in a counted cell was in the range of 100–300). Figures 9a and 9b are the axially, azimuthally, and time-averaged (over 20 h) axial and radial velocity profiles. One can see from the figures that solid particles move in the organized pattern, upward in the center and downward near the wall of the column. The maximum upflow velocity is about 0.47 mm/s, occurring near the center of the column, while the maximum downflow velocity is about 0.57 mm/s, occurring at a dimensionless radius of 0.78 (Figure 9a). The flow inversion point is at dimensionless radius of about 0.42. This flow pattern is similar to those observed in gas–solid fluidized beds (Moslemian et al., 1992), in bubble columns (Devanathan et al.; Franz et al., 1984; Menzel et al., 1990; Mudde et al., 1997; Chen et al., 1998a, 1998b), in liquid–solid and gas–liquid–solid fluidized beds (Limtrakul, 1996; Larachi et al., 1995), and in liquid–solids risers (Roy et al., 1997). Compared to the axial velocity, the radial velocity of the particle is much smaller, as is evident from Figure 9b, with a maximum velocity of 0.067 mm/s. In the first approximation, it can be assumed that solid particles in the bed are mostly moving in the axial direction at the employed operating conditions.

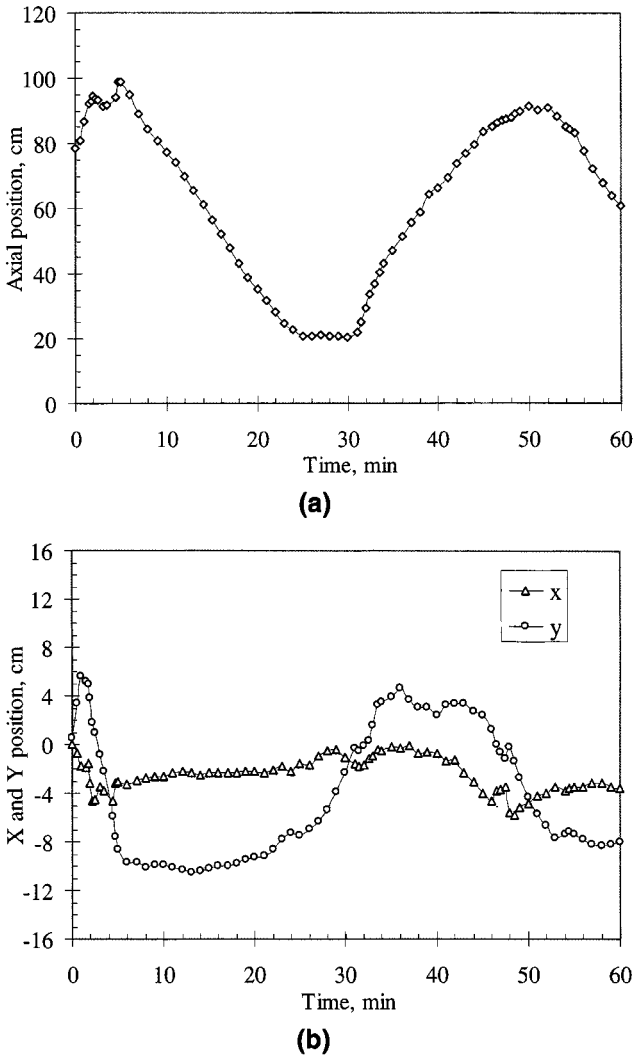

Figure 8. Particle trajectories.

$U_g = 2$ cm/s, $U_l = 0.3$ cm/s, air–water + ethanol–alumina, two-phase upflow, particle original position: center of the column and 20 cm below the solids free surface. Trajectory in (a) *z* direction; (b) *x* and *y* directions.

Figure 10 presents the side view of the azimuthally averaged two-dimensional velocity vector plot. The arrows represent the direction and magnitude of the velocity vectors. It should be noted that in some regions/positions there are no arrows since the radioactive particle never visited those regions/positions. Therefore the velocities (directions and magnitudes) are unknown in these regions/positions, which does not imply that the velocities are zero. From the vector plot, one can see that the radioactive particle was traveling axially and radially throughout the bed except at the bottom (up to 20 cm above the distributor).

Experimental liquid velocity for incipient particle migration vs. predicted minimum liquid fluidization velocity

Based on the results discussed earlier, the superficial liquid velocity of 0.3 m/s can be considered as the liquid veloc-

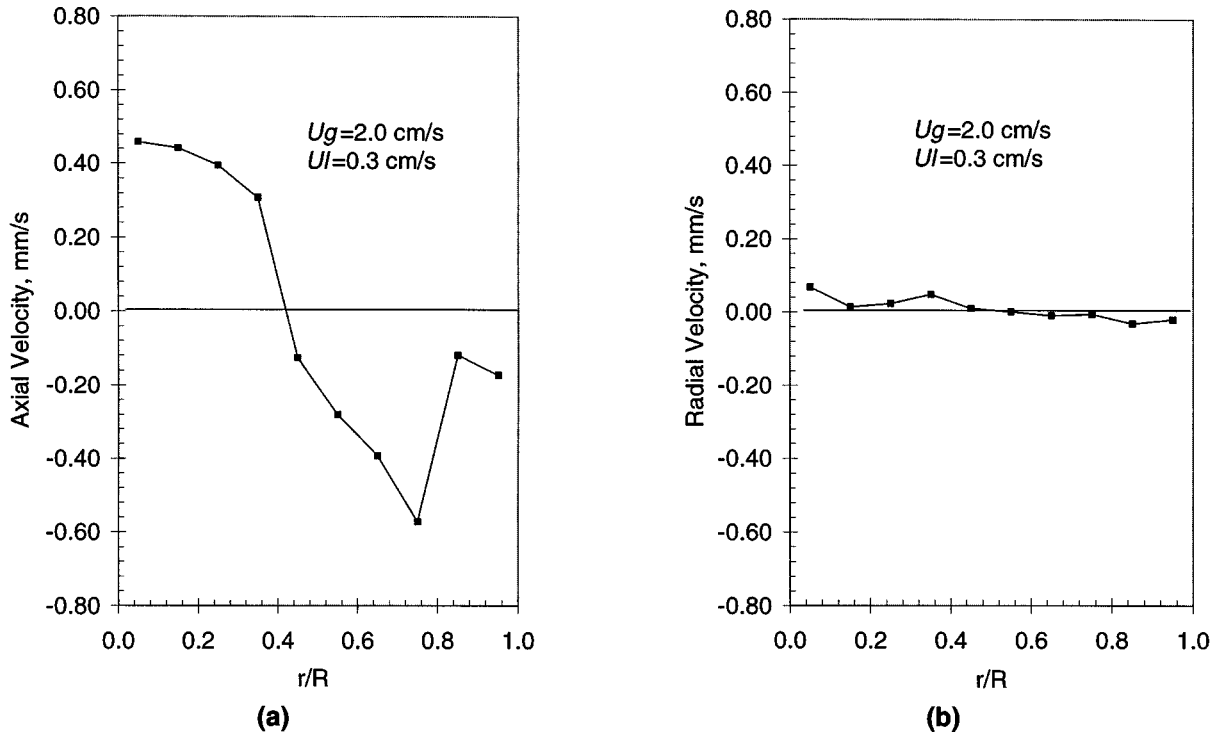

Figure 9. Axially, azimuthally, and time-averaged particle axial and radial velocities.

$U_g = 2$ cm/s, $U_l = 0.3$ cm/s, air–water + ethanol–alumina, two-phase upflow: (a) axial velocity; (b) radial velocity.

ity for incipient migration of the particles ($U_{l,0}$) at a superficial gas velocity of 1.7 cm/s. At these velocities the bed can be still considered as packed, since observed bed expansion is negligible. However, the velocities of the gas and liquid phases is adequate to transmit a sufficient amount of kinetic energy to the solid particles, which causes them to vibrate (based on visual observation and CARPT results) and migrate, organized in the recirculation pattern throughout the bed (based on CARPT data). Further increase of the gas and liquid velocities will increase the bed expansion toward the minimum fluidization velocity ($U_{l,mf}$). The existing models and correlations are used to evaluate the $U_{l,mf}$ for the studied system (air–water + ethanol–alumina). Three different models were chosen for the calculation, the phenomenological model proposed by Zhang et al. (1995), the empirical correlation proposed by Bloxom et al. (1975), and the two artificial neural network (ANN) approaches proposed by Larachi et al. (2000). It was found that the phenomenological model of Zhang et al. (1995) failed for the current system because the calculated gas void fraction per unit of the porous volume at minimum fluidization is greater than unity. The empirical correlation of Bloxom et al. (1975) yielded a value for $U_{l,mf}$ of 0.4 cm/s, which is a little higher than the experimentally observed $U_{l,0}$ (0.3 cm/s). The dimensional ANN approach (Larachi et al., 2000) under predicted $U_{l,mf}$ (0.05 cm/s is much smaller than $U_{l,0}$). In contrast, the dimensionless ANN model predicted a higher value of $U_{l,mf}$ (1.25 cm/s) than that predicted by the Bloxom et al. (1975) model (0.4 cm/s) and than the $U_{l,0}$ value (0.3 cm/s). Since neither the bed expansion nor pressure drop were monitored, reasonable comparison between experimental and calculated $U_{l,mf}$ was not possible and is beyond the scope of this work. It should be pointed out that most of the reported experimental data on $U_{l,mf}$ referred to the beds of diameter less than 17.15 cm, which is much smaller than the diameter of the bed used in the present study (30.5 cm). In addition, none of the reported models/correlations take the design of the distributor into account, which proved to be important to the fluid distribution and flow pattern in the bed, as concluded from this study.

Conclusions

CT scans were conducted to evaluate the cross-sectional gas holdup distribution in the air–water–solids (alumina particles of 3.2-mm diameter) system at a superficial gas velocity of 2.0 cm/s and superficial liquid velocity of 0.3 cm/s, and it was found that at these conditions despite particle migration the solids are still essentially in a packed bed (due to the negligible bed expansion). The gas-holdup distribution obtained with distributor II (perforated plate with 96 holes of 1 mm in diameter uniformly distributed in triangular pattern; open area of 0.1%) with a cross-shaped sparger in the plenum is relatively uniform with gas holdup of about 0.11 in the center and 0.09 near the wall of the column. The cross-sectional averaged gas and solid holdups in the bed are about 0.095 and 0.66, respectively.

In the air–water–ethanol (10% ethanol by weight) –alumina system, at a superficial gas velocity of 1.7 cm/s and superficial liquid velocity of 0.3 cm/s, solids particles in the bed start to move and travel long distances. These gas and

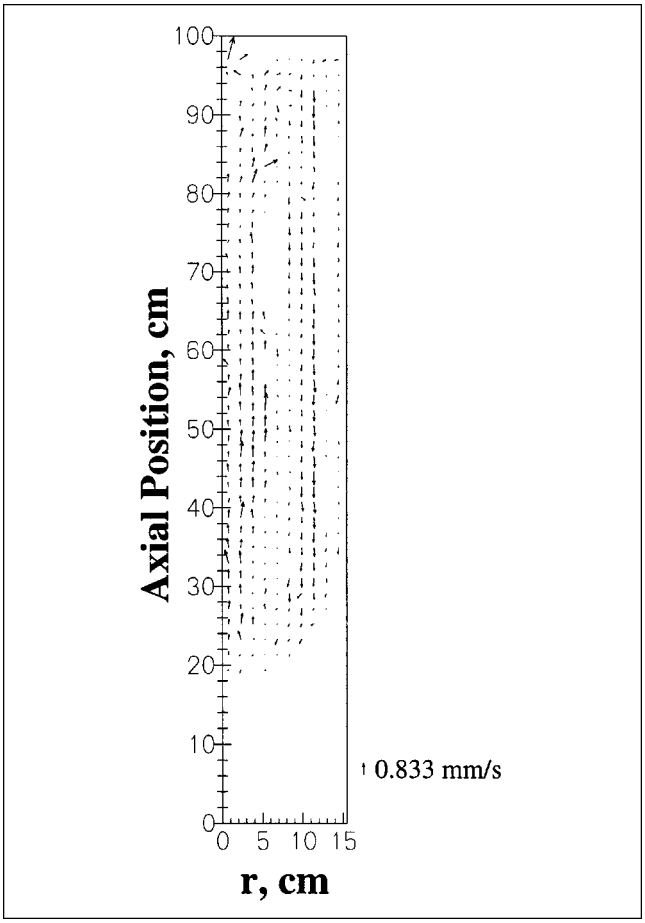

Figure 10. 2-D velocity vector of azimuthally and time-averaged particle velocity.

$U_g = 2$ cm/s, $U_l = 0.3$ cm/s, air–water + ethanol–alumina, two-phase upflow.The radioactive particle never visited the regions/positions where there are no arrows.

liquid velocities correspond to the velocities for the incipient particle migration, but not to the minimum fluidization conditions for this system. In the air–water–ethanol (10% ethanol by weight) – alumina system, at a superficial gas velocity of 2.0 cm/s and superficial liquid velocity of 0.3 cm/s, the solid particles in the bed exhibit significant axial movement throughout the column with upflow in the center and downflow near the wall of the column. The time-averaged maximum upward and downward velocities of the particles are about 0.47 mm/s and 0.57 mm/s, respectively. The radial movement of the solids particles is negligible. Thus CARPT and CT can be used to provide a valuable database for establishing a correlation for the onset of incipient migration in two- and three-phase flow packed beds.

Some of the existing models/correlations for the minimum liquid fluidization velocity in gas–liquid–solid three-phase fluidized beds predict a proper trend of higher minimum liquid fluidization velocity than the determined superficial liquid velocity for the incipient particle migration. However, further study is needed to systematically and quantitatively compare experimentally measured and predicted minimum liquid fluidization velocity and the liquid velocity for the incipient particle migration.

Acknowledgment

The authors acknowledge the financial support for conducting this study provided by Chevron Research and Technology Company.

Notation

A = net attenuation

$A_{l,ij}$, $A_{g-s,ij}$, $A_{l-s,ij}$ $A_{g-l-s,ij}$ = net attenuation of pure liquid, gas–solid, liquid–solid and gas–liquid–solid phase in the ij pixel

D = column diameter, cm

I = detected radiation

I_0 = incident radiation

l = path length

L = total path length through the composite material

L_{ij} = total path length through the ij pixel

R = radius of column, cm

r = radial position, cm

T = transmission ratio

U_g = superficial gas velocity, cm/s

U_l = superficial liquid velocity, cm/s

$U_{l,0}$ = superficial liquid velocity for the incipient migration of solid particles, cm/s

$U_{l,mf}$ = superficial liquid velocity at minimum fluidization, cm/s

Greek letters

ϵ = phase holdup or phase volume fraction

ϵ_1, ϵ_2 = holdup of phase 1 and phase 2

$\epsilon_{g,ij}$, $\epsilon_{l,ij}$, $\epsilon_{s,ij}$ = holdup of gas, liquid and solids in the ij pixel

μ = mass attenuation coefficient, g/cm^2

μ_1, μ_2 = attenuation coefficient of phase 1 and phase 2, g/cm^2

μ_g, μ_l, μ_s = attenuation coefficient of gas, liquid and solid phase, g/cm^2

ρ = density of material, g/cm^3

ρ_1, ρ_2 = density of phase 1 and 2, g/cm^3

ρ_g, ρ_l, ρ_s = density of gas, liquid and solid phase, g/cm^3

Subscripts

1, 2 = phases 1 and 2

Literature Cited

Bascoul, A., J. P. Couderc, and H. Delmas, "Solids Motion in Liquid-Solid Fluidization (Mouvement des particules solides en fluidisation liquide-solide)," *Chem. Eng. J.*, **52**, 235 (1993).

Bloxom, V. R., J. M. Costa, J. Herranz, G. L. MacWilliam, and S. R. Roth, "Determination and Correlation of Hydrodynamic Variables in a Three-Phase Fluidized Bed," MIT Rept. N219, Oak Ridge National Laboratory, Oak Ridge, TN (1975).

Chaouki, J., F. Larachi, and M. P. Duduković, "Noninvasive Tomographic and Velocimetric Monitoring of Multiphase Flows," *Ind. Eng. Chem. Res.* **36**, 4476 (1997).

Chen, R. C., and L.-S. Fan, "Particle Image Velocimetry for Characterizing the Low Structure in Three-Dimensional Gas–Liquid–Solid Fluidized Beds," *Chem. Eng. Sci.*, **47**, 3615 (1992).

Chen, J., P. Gupta, M. H. Al-Dahhan, M. P. Duduković, and B. A. Toseland, "Gas Holdup Distributions in Large Diameter Bubble Columns Measured by Computed Tomography," *Flow Meas. Instrum.*, **9**, 91 (1998).

Chen, J., F. Li, S. Degaleesan, P. Gupta, M. H. Al-Dahhan, M. P. Duduković, and B. A. Toseland, "Fluid Dynamic Parameters in Bubble Columns with Internals," *Chem. Eng. Sci.*, **54**, 2187 (1999).

Degaleesan, S., "Fluid Dynamic Measurements and Modeling of Liquid Mixing in Bubble Columns," PhD Thesis, Washington Univ. in St. Louis, St. Louis, MO (1997).

Degaleesan, S., M. P. Duduković, B. A. Toseland, and B. L. Bhatt, "A Two-Compartment Convective-Diffusion Model for Slurry Column Reactors," *Ind. & Eng. Chem.*, **36**, 4670 (1997).

Devanathan, N., D. Moslemian, and M. P. Duduković, ''Flow Mapping in Bubble Columns Using CARPT,'' *Chem. Eng. Sci.*, **45**, 2285 (1990).
Devanathan, N., ''Investigation of Liquid Hydrodynamics in Bubble Columns via Computer Automated Radioactive Particle Tracking,'' PhD Thesis, Washington Univ. in St. Louis, St. Louis, MO (1991).
Franz, K., T. Borner, H. J. Kantorek, and R. Buchholz, ''Flow Structures in Bubble Columns,'' *Ger. Chem. Eng.*, **7**, 365 (1984).
Gross, E. W., and J. M. Kuhlman, ''Three-Component Velocity Measurements in a Turbulent Recirculating Bubble-Driven Liquid Flow,'' *Int. J. Multiphase Flow*, **18**, 413 (1992).
Halow, J. S., ''Electrical Capacitance Imaging of Fluidized Beds,'' *Non-Invasive Monitoring of Multiphase Flows*, Chap. 9, J. Chaouki, F. Larachi, and M. P. Duduković, eds, Elsevier, Amsterdam, p. 263 (1997).
Kantzas, A., ''Computation of Holdups in Fluidized and Trickle Beds by Computer-Assisted Tomography,'' *AIChE J.*, **40**, 1254 (1994).
Kumar, B. S., ''Computer Tomographic Measurements of Void Fraction and Modeling of the Flow in Bubble Columns,'' PhD Thesis, Florida Atlantic Univ., Boca Raton (1994).
Kumar, B. S., D. Moslemian, and M. P. Dudukovic, ''A Gamma Ray Tomographic Scanner for Imaging Void Fraction Distribution in Bubble Columns,'' *Flow Meas. Instrum.* **6**, 61 (1995).
Kumar, S. B., D. Moslemian, and M. P. Duduković, ''Gas Holdup Measurements in Bubble Columns Using Computed Tomography,'' *AIChE J.*, **43**, 1414 (1997).
Larachi, F., G. Kennedy, and J. Chaouki, ''3-D Mapping of Solids Flow Fields in Multiphase Reactors with RPT,'' *AIChE J.*, **41**, 439 (1995).
Larachi, F., I. Iliuta, O. Rival, and B. P. A. Grandjean, ''Prediction of Minimum Fluidization Velocity in Three-Phase Fluidized-bed Reactors,'' *Ind. Eng. Chem. Res.*, **39**, 563 (2000).
Limtrakul, S., ''Hydrodynamics of Liquid Fluidized Beds and Gas-Liquid Fluidized Beds,'' PhD Thesis, Washington Univ. in St. Louis, St. Louis, MO (1996).
Menzel, T., T. in der Weide, O. Staudacher, O. Wein, and U. Onken, ''Reynolds Shear Stress for Modeling of Bubble Column Reactors,'' *Ind. Eng. Chem. Res.*, **29**, 988 (1990).
Moslemian, D., N. Devanathan, and M. P. Duduković, ''Radioactive Particle Tracking Technique for Investigation of Phase Recirculation and Turbulence in Multiphase Systems,'' *Rev. Sci. Instrum.*, **63**, 4361 (1992).
Mudde, R. F., J. S. Groen, and H. E. A. van den Akker, ''Liquid Velocity Field in a Bubble Column: LDA Experiments,'' *Chem. Eng. Sci.*, **52**, 4217 (1997).
Mudde, R. F., W. K. Harteveld, H. E. A. van den Akker, T. H. J. J. van der Hagen, and H. van Dam, ''Gamma Radiation Densitometry for Studying the Dynamics of Fluidized Beds,'' *Chem. Eng. Sci.*, **54**, 2047 (1999).
Roy, S., J. Chen, S. Kumar, M. H. Al-Dahhan, and M. P. Duduković, ''Tomography and Particle Tracking Studies in a Liquid-Solid Riser,'' *Ind. Eng. Chem. Res.*, **36**, 4666 (1997).
Shollenberger, K. A., J. R. Torczynski, D. R. Adkins, T. J. O'Hern, and N. B. Jackson, ''Gamma-Densitometry Tomography of Gas Holdup Spatial Distribution in Industrial Scale Bubble Columns,'' *Chem. Eng. Sci.*, **52**, 2037 (1997).
Yang, Y. B., N. Devanathan, and M. P. Duduković, ''Liquid Backmixing in Bubble Columns via Computer-Automated Radioactive Particle Tracking (CARPT),'' *Exp. Fluids*, **16**, 1 (1993).
Yates, J. G., D. J. Cheesman, and Y. A. Sergeev, ''Experimental Methods in Fluidized Research,'' *Int. J. Multiphase Flow*, **20**, 297 (1994).
Yates, J. G., ''Experimental Observations of Voidage in Gas Fluidized Beds,'' *Non-Invasive Monitoring of Multiphase Flows*, Chap. 4, J. Chaouki, F. Larachi, and M. P. Duduković, eds., Elsevier, Amsterdam, p. 141 (1997).
Zhang, J., N. Epstein, J. R. Grace, and J. Zhu, ''Minimum Fluidization Velocity of Gas−Liquid Fluidized Beds,'' *Trans. Inst. Chem. Eng.*, **73**, 347 (1995).

Manuscript received Aug. 9, 1999, and revision received Oct. 19, 2000.